ACS OMEGA

ACS AUTHORCHOICE

http://pubs.acs.org/journal/acsodf

Article

Enhanced Thermoelectric Properties of Poly(3-hexylthiophene) through the Incorporation of Aligned Carbon Nanotube Forest and Chemical Treatments

Saeed Mardi, Khabib Yusupov, Patricia M. Martinez, Anvar Zakhidov, Alberto Vomiero,* and Andrea Reale*

Cite This: https://dx.doi.org/10.1021/acsomega.0c02663

Read Online

ACCESS | Metrics & More | Article Recommendations | Supporting Information

ABSTRACT: Carbon nanotube/polymer composites have recently received considerable attention for thermoelectric (TE) applications. The TE power factor can be significantly improved by forming composites with carbon nanotubes. However, the formation of a uniform and well-ordered nanocomposite film is still challenging because of the creation of agglomerates and the uneven distribution of nanotubes. Here, we developed a facile, efficient, and easy-processable route to produce uniform and aligned nanocomposite films of P3HT and carbon nanotube forest (CNTF). The electrical conductivity of a pristine P3HT film was improved from ~10^{-7} to 160 S/cm thanks to the presence of CNTF. Also, a further boost in TE performance was achieved using two additives, lithium bis(trifluoromethanesulfonyl) imide (LiTFSI) and *tert*-butylpyridine. By adding the additives to P3HT, the degree of interchain order increased, which facilitated the charge transport through the composite. Under the optimal conditions, the incorporation of CNTF and additives led to values of the Seebeck coefficient, electrical conductivity, and power factor up to rising 92 μV/K, 130 S/cm, and 110 μW/m K^2, respectively, at a temperature of 344.15 K. The excellent TE performance of the hybrid films originates from the dramatically increased electrical conductivity and the improved Seebeck coefficient by CNTF and additives, respectively.

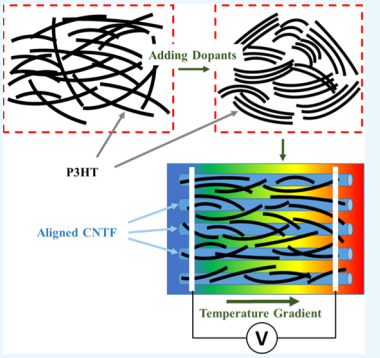

INTRODUCTION

Because the problem of increasing carbon emissions and renewable energy sources is becoming more urgent, the importance of environmentally friendly alternative energy sources has become more necessary.[1] Thermoelectric (TE) materials have great potential as heating pumps and power generators, which can enable the direct conversion between thermal and electrical energy without any moving mechanical components.[2] The performance of TE materials is evaluated by a figure-of-merit, given by $ZT = S^2\sigma T/k$, where S, σ, T, and k are the Seebeck coefficient (μV/K), the electrical conductivity (S/m), the absolute temperature (K), and the thermal conductivity (W/m K), respectively. In order to maximize ZT, it is necessary to have a high Seebeck coefficient and electrical conductivity, as well as a low thermal conductivity. The ideal TE material would be a "phonon−glass, electron−crystal" (PGEC), which conducts heat poorly, just like an amorphous glass, but possesses a high electrical conductivity, just like a crystalline material.[3]

However, these parameters (S and σ) are highly negatively correlated. This makes it difficult to optimize the figure-of-merit. The measure of thermal conductivity is challenging especially in thin films because of heat conduction through the substrate, thermal contact resistance, and radiation loss.[4] Therefore, the power factor, which is proportional to the output power of the TE device, can be used as a preliminary fundamental parameter to evaluate the performance of TE materials.[5]

TE materials can be divided into three categories, depending on their temperature range of operation: low temperature, 250−500 K (mainly Bi_2Te_3-based), medium temperature, 500−900 K (mainly PbTe-based), and high temperature, above 900 K (mainly SiGe-based). Even though the temperature range of most industrial waste heat sources is between 500 and 900 K, it should be emphasized that most of waste heat is released at temperatures below 400 K.[6] The Bi_2Te_3-based materials are usually known to be the only inorganic TE materials with good TE properties at room temperature. However, the inorganic TE materials are associated with several drawbacks, such as scarcity in nature, high cost of production, toxicity, and difficulty in processing.[7] On the other hand, the conducting polymers have a low thermal conductivity (0.1−0.5 W/m K), high chemical stability, low density, flexibility, nontoxicity, and low cost, easily synthesiz-

Received: June 13, 2020
Accepted: September 4, 2020

able, and their properties can be suitably tuned.[6] All these advantages make conducting polymers promising candidates for new-generation TE devices close to room temperature.

Among various conducting polymers, poly(3-hexylthiophene) (P3HT) is one of the most extensively explored organic materials for TE applications.[8,9] The interest in P3HT stems from its desirable intrinsic characteristics such as excellent solution processability, chemical and thermal stability, and high field-effect mobility.[10,11] Interestingly, it has a high tolerance against energetic particle irradiations, which could be suitable for space applications.[12] Moreover, P3HT is soluble in a variety of common organic solvents, including nonchlorinated ones. This feature makes it suitable for large-area processing techniques such as spray-printing,[13] bar-coating,[14] and inkjet-printing.[15] However, it suffers from low electrical conductivity and improving this outcome has proved to be challenging. To address this issue, various routes are being explored, such as changing its molecular configuration,[16] using different solvents,[5] adding different dopants,[17] and tuning its crystallinity and molecular weight.[18,19] The most efficient approach to improve the electrical conductivity of P3HT is to use the iron salt dissolved in nitromethane. It could improve its conductivity up to 250 S/cm with a Seebeck coefficient of 40 μV/K.[18] However, based on its MSDS, nitromethane is not a green solvent and is categorized as a dangerous solvent because of its explosive properties.

Recently, carbon nanotubes (CNTs) got a lot of attention as a filler for organic TE materials. The incorporation of CNTs into polymers dramatically increases the electrical conductivity by creating a network of CNTs in the composite, while keeping the thermal conductivity of the composite nearly constant relative to the polymer regardless of whether CNTs are added. The low thermal conductivity of the composite could be explained by the existence of the filler/polymer interfaces. These interfaces increase the phonon scattering rate by suppressing the phonon transport and ensuring that the composite has a low thermal conductivity.[13,20] In this respect, several studies have reported that the composite of CNTs and organic materials exhibit high electrical conductivity, without increasing significantly the thermal conductivity.[9,21−23] A similar behavior was also reported for the Seebeck coefficient. Because of the interdependence of S and σ, the addition of dopant increases the electrical conductivity and decreases the Seebeck coefficient.[24] However, the phase-separated CNT-rich and polymer-rich regions in the composites could enable a simultaneous increase in electrical conductivity and the Seebeck coefficient.[25]

The CNT-based composites are usually prepared by physically blending the CNTs and P3HT into a solvent or in situ polymerization.[14,26] One of the drawbacks of using those approaches is the random dispersion of CNTs within the polymer. Moreover, because of the high surface area of the CNTs and strong van der Waals attractive forces between them, CNTs might agglomerate within the polymer matrix. These drawbacks negatively affect the electrical properties.[27] One possible approach to overcome these drawbacks is directly using CNT arrays in which CNTs are already aligned.[28] Here, for the first time, we used a vertically aligned, highly ordered, CNT forest (CNTF) as a filler to improve the TE properties of P3HT. Additionally, the two additives, LiTFSI and *tert*-butylpyridine (TBP), were used to improve the electrical properties of the polymer film. The comparison among different formulations shows that the incorporation of CNTF alongside the presence of additives significantly improves the power factor up to 110 μW/m K. These outstanding results provide an effective approach to produce high-performance TE materials, by combining the properties of CNTF (high electrical conductivity and ordering) and P3HT (low thermal conductivity and high Seebeck coefficient). This approach could be developed to make large-area and flexible TE materials based on P3HT.

RESULTS AND DISCUSSION

Scheme 1 illustrates the sample preparation process, and Figure 1 compares the top-view morphologies of the different

Scheme 1. Sample Preparation Process for Making the P3HT/CNTF Composite[a]

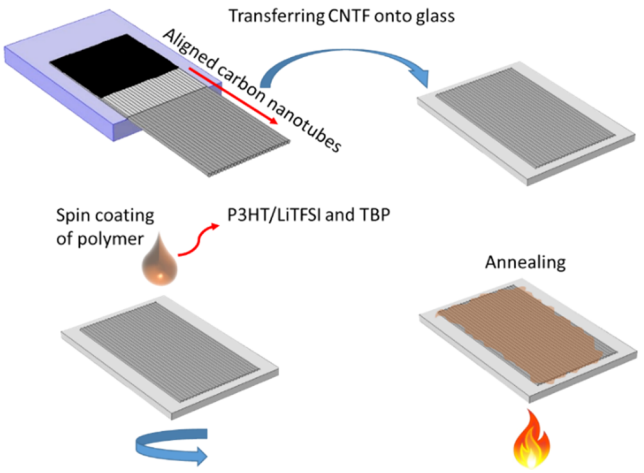

[a]First, CNTF was pulled from the plate and transferred onto the glass. Then, the solution was spin-coated on top of that. Finally, the film was annealed at 150 °C.

samples. As mentioned in the Experimental Section, first, the CNTF was transferred onto the glass (the bare CNTF is shown in the inset of Figure 1b). Then, P3HT solutions were spin-coated. The pristine polymer is shown in Figure 1a. As shown in Figure 1b, the CNTs are aligned in the polymer matrix; the comparison between bare CNTF and P3HT/CNTF 0 illustrates that the deposition of the polymer does not change the orientation of CNTF. The addition of the additives makes the surface rougher, and new grains of the polymer appear on the surface (labeled by red arrows and red shapes in the SEM images). Aggregates like those are commonly observed in polymer films by adding LiTFSI dissolved in acetonitrile.[29] Juarez-Perez et al.[30] investigated these aggregates in the polymer film, and it was proved that they are the aggregates of the LiTFSI salt. Consequently, CNTs in the doped samples are not as visible as in Figure 1a.

The comparison between the samples with and without CNTF shows that the composite films have smaller aggregates. Therefore, it shows that introducing CNTF may have led to a homogeneous distribution of LiTFSI within the polymer. Another aspect of the effect of additives was the thickness. The thicknesses of samples were increased by increasing the amount of additives, as reported in Table S1. Raman spectroscopy can be conveniently used to probe the structure of polymer nanocomposites,[31] and we applied it to investigate the structure of conjugated carbon bonds. Raman spectra of P3HT and P3HT/CNTF layers with different additive

https://dx.doi.org/10.1021/acsomega.0c02663
ACS Omega XXXX, XXX, XXX−XXX

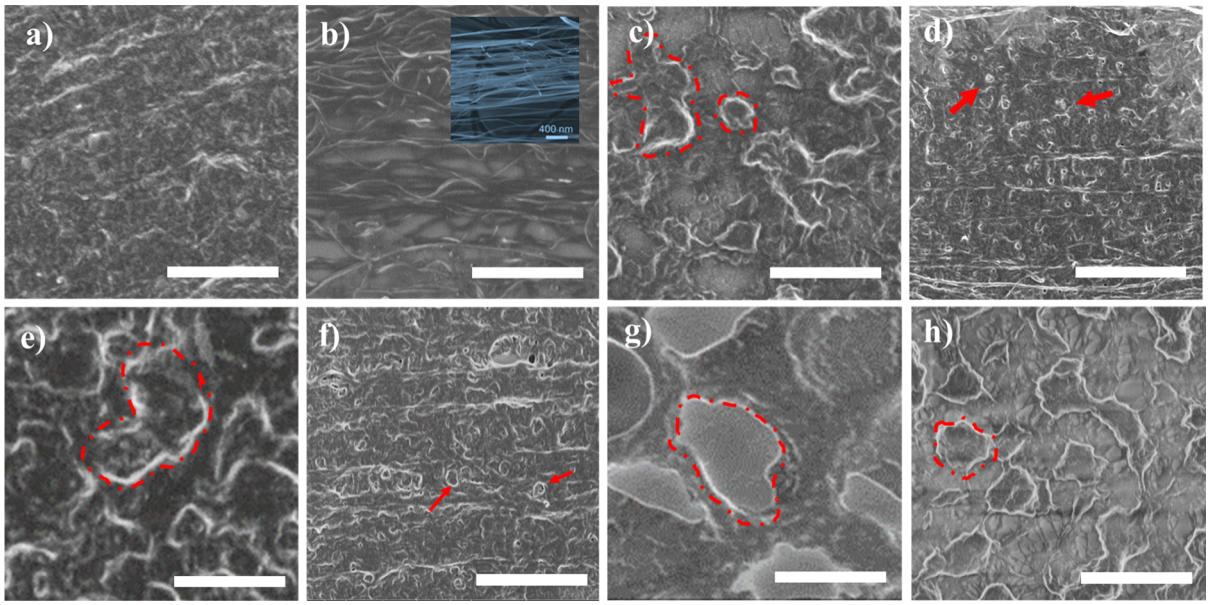

Figure 1. Top-view FE-SEM images of pure P3HT and P3HT/CNTF composite films with different additive ratios. P3HT 0 and P3HT/CNTF 0 (a,b); P3HT 1 and P3HT/CNTF 1 (c,d); and P3HT 2 P3HT/CNTF 2 (e,f) and P3HT 3 P3HT/CNTF 3 (g,h). The inset image in (b) is bare CNTF on the glass. Markers in the main images correspond to 2 μm. The red shapes and arrows represent polymer agglomerates on the surface because of the additives.

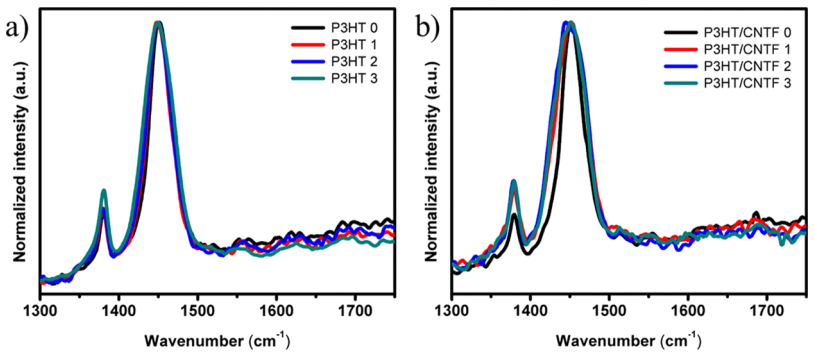

Figure 2. Raman spectra of (a) P3HT and (b) P3HT/CNTF with different additive ratios.

contents are presented in Figure 2a,b, respectively. The Raman spectrum of pure CNTFs on the glass is demonstrated in Figure S2. Raman peaks at 1349 and 1580 cm^{-1} correspond to the defect band (D-band) and graphite band (G-band) from the CNTF layer, respectively. The high-intensity ratio I_G/I_D of the G-band and D-band of the Raman shift confirms the high quality of CNTFs.[32] The Raman spectrum of P3HT (Figure 2a) contains two strong peaks at 1448 and 1379 cm^{-1}, which are assigned to the C−C and the C═C skeletal stretching vibrations, respectively.[33]

The Raman spectra of different samples with different dopant contents are similar, suggesting that the structure of P3HT remains unaltered after adding the additives. The Raman spectra for the composite samples with different dopant levels are reported in Figure 2b. The peaks of the CNTF cannot be seen in the Raman spectra of the composites because they are masked by peaks of P3HT.

In planar conjugated polymers such as P3HT, there is an anisotropy in charge transport. The highest charge transport is along the conjugated backbone (*c*-axis) because of the covalently linked conjugated units. Along the $\pi-\pi$ stacking axis, the charge transport is slower (*b*-axis), and the slowest charge transport happens along the lamellar stacking axis (*a*-axis) (see Figure 3a). Therefore, the charge transfer through a film requires a percolated network of conjugation.[34,35] Therefore, improvement in the interchain order along the conjugated backbone could improve the charge transport.

Chang et al.[36] investigated the correlation of interchain interaction and the field-effect mobility in different molecular weights of P3HT. Their results showed that upon increasing the molecular weight, the interchain order and the field-effect mobility increased. UV−vis absorption spectroscopy was conducted in order to study the typical behavior related to $\pi-\pi^*$ absorption transitions, positioned at peaks ∼607, ∼558, and ∼525 nm. The absorption peaks at 525 nm and 607 nm give information on the degree of conjugation of the P3HT chains and the degree of the interchain order.[10] The peak at 607 nm corresponds to the formation of an exciton delocalized over multiple P3HT chains, and its intensity reflects the crystalline order of the polymer.[37,38] Figure 3b,c shows the normalized UV−vis absorbance spectra of the P3HT and P3HT/CNTF layers with different amounts of additives, respectively. As shown in Figure 3b, the increase in the peak intensity at 607 nm shows that the addition of additives

https://dx.doi.org/10.1021/acsomega.0c02663
ACS Omega XXXX, XXX, XXX−XXX

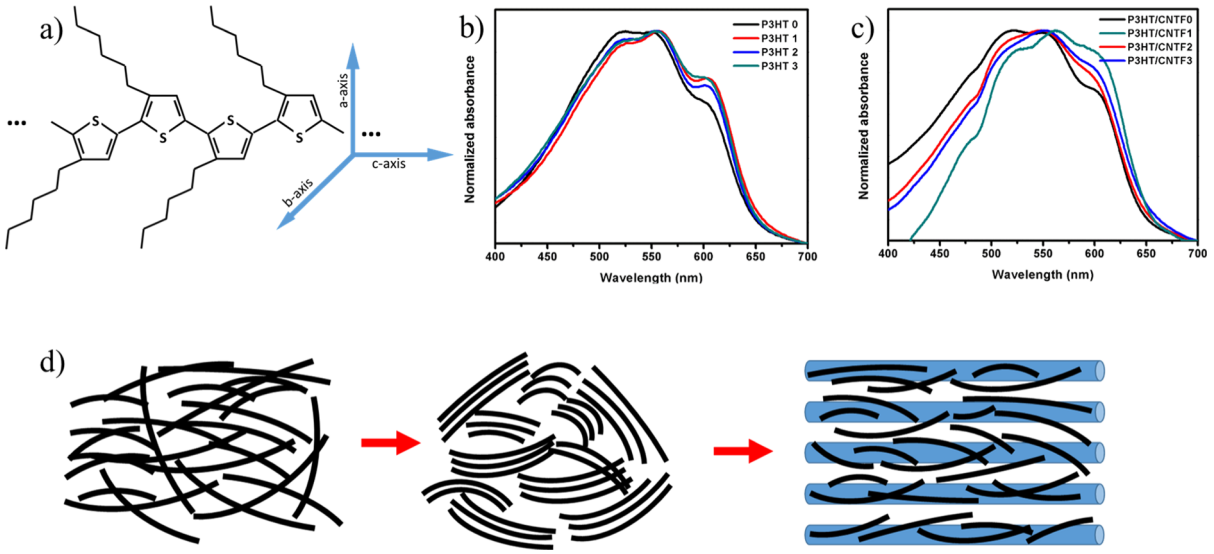

Figure 3. (a) Structure of the P3HT polymer and three main axes, in which anisotropic charge transport occurs: the *a* and *b* axes in the polymer plane are the lamellar stacking and conjugated backbone directions, respectively, and the *c* axis vertical to polymer plane is the p−p stacking axis. The normalized UV−vis absorbance spectra of (b) P3HT and (c) P3HT/CNTF layers with different additive ratios deposited on the glasses. (d) Microstructure of the P3HT polymer and its evolution after the addition of the additives and incorporation of CNTF.

increases the interchain order. Increasing the interchain order facilitates the charge transport in the layer. According to the reported literature, the presence of LiTFSI increases the density of charge carriers, and TBP prevents the formation of individual and isolated aggregates of LiTFSI.[30,39−41] Therefore, TBP helps to keep the distribution of LiTFSI homogeneous and ensures the uniform electrical properties of the film.[30] To investigate the effect of TBP in our formulation, the solutions of P3HT 1 and P3HT 2 both without TBP were prepared and the corresponding films were deposited under similar conditions to the prior samples of P3HT 1 and P3HT 2 with TBP. The images of the obtained samples with and without TBP are compared in Figure S3. The addition of TBP significantly improved the quality of the films. As shown in Figure S3c,d, the P3HT 1 and P3HT 2 films without TBP are not homogeneous and include large holes. In addition, TBP has a higher boiling point compared to the solvents which might help to improve the morphology of the nanocomposites. The addition of high boiling additives to the polymer solutions usually improves the structure and morphology of the polymers.[42,43]

The electrical conductivity of different samples increases with additive concentrations, consistently with our assumption. The order of magnitude of electrical conductivity P3HT 0, P3HT 1, P3HT 2, and P3HT 3 at room temperature was about $\sim 10^{-5}$, $\sim 10^{-3}$, $\sim 10^{-1}$, and ∼10 S/m, respectively. However, for the sample with the highest level of additive, the intensity of the peak at 607 nm slightly decreases, suggesting that the interchain ordering is slightly reduced. This could be attributed to the fact that an excessive amount of additive cannot be uniformly distributed within the P3HT matrix, and the polymer chains would be unpacked and inhomogeneous because of the formation of large grains. This morphology change might decrease the electron delocalization along the polymer chain, affecting carrier mobility. Figure 3c presents the normalized UV−vis spectra of P3HT/CNTF. The comparison of the peak intensity at 607 nm shows a similar trend of the interchain order in the composite layers. The additives improved the crystalline order. Interestingly, a red shift of the overall absorbance was observed for the P3HT/CNTF 1. The red shift is related to the stronger interaction and charge transfer between P3HT and CNTF in P3HT/CNTF 1.[38,44,45] However, the peak shifts in the other composite samples are smaller compared to P3HT/CNTF 1. The SEM images had already shown that the larger grains on the surface appeared as a result of increasing the amounts of additives. These grains might reduce the effective interpenetration between CNTF and the polymer. Therefore, the polymer could not cover the CNTF conformally, just as had been the case when the amount of additives was lower. Therefore, the interaction of CNTF and the polymer was decreased. Figure S4 shows the normalized UV−vis spectra for all the samples. The highest intensity of the peak at 607 nm belongs to P3HT/CNTF 1.

For all of the samples with different additive contents, the intensity of the peak at 607 nm is increased by the addition of CNTF. This confirms that CNTF increases the interchain order in the polymer chain, which contributes to the charge transfer in the composite film, even though we did not use any chemical reaction for making the composite. This phenomenon could probably be attributed to the fact that the torsional rotations of the thiophene rings of the polymer are reduced because of the ordering effect from CNTFs.[38,44] Therefore, the overlap of the wave functions of the chains with their nearest neighbors has been increased, enhancing the interchain interactions and conjugation length.[37,38,46−48] We suggest that by having added the additives and incorporating CNTFs, the interchain order and the electron delocalization in the polymer chain were improved. These processes facilitate the propagation of electrons along the $\pi-\pi$ conjugated region and might lead to higher carrier mobility.[16,49] The effect of additives and CNTF is schematically shown in Figure 3d. The black lines represent the conjugated backbone direction. The left, middle, and right pictures show pristine P3HT, P3HT with additives, and the nanocomposite of P3HT/CNTF, respectively. The introduction of additives and incorporating CNTF improve the ordering and alignment of polymer chains. This makes a better network for charge transport. For further investigation of the interaction between CNTF and P3HT, the

https://dx.doi.org/10.1021/acsomega.0c02663
ACS Omega XXXX, XXX, XXX−XXX

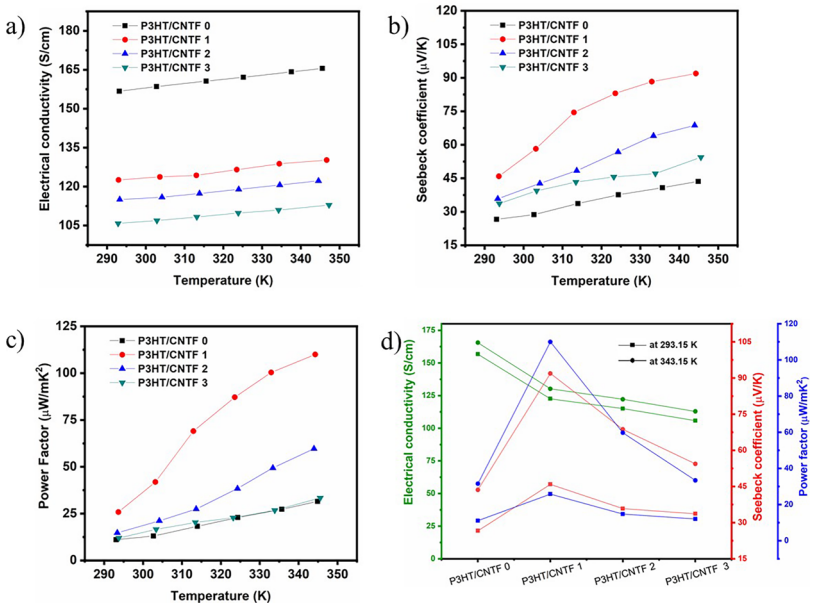

Figure 4. (a) Electrical conductivity, (b) Seebeck coefficient, and (c) power factor of P3HT 3 and P3HT/CNTF with different amounts of additives vs temperature; (d) summarizing results for the different samples.

optical energy band gaps were determined by UV−vis absorption onset in the thin films and the results have been shown in Figure S5. Adding the additives slightly reduced the band gap of the P3HT films. The incorporation of CNTF also lowers the band gap. Interestingly, in the case of P3HT/CNTF 1, the band gap decreased more than other composites. As was explained in the previous paragraph, this might be related to the morphology change in the polymer and a loss of an effective connection between polymer chains.

To further investigate the effect of additives, the XRD patterns were recorded and displayed in Figure S6. The XRD pattern of the pristine P3HT did not show any specific peaks, which demonstrated random polymer chain arrangements in the pristine P3HT. The doped samples (P3HT 1 and P3HT 2) show two sharp peaks at 8 and 16.2°, which correspond to the lattice planes (200) and (300) of P3HT, respectively.[16] The (*h*,0,0) features corresponded to the lamellar stacking axis in the polymer (*a*-axis). Increasing the additive concentration results in stronger peaks and their shift to higher angles, which corresponds to the reduction of the lamellae distance. An increase in the lamellae distance in the polymer might improve the interchain interaction leading to higher crystallite dimensionality.[50] However, in the P3HT 3 sample, the crystallinity of the P3HT film is reduced possibly because of the inhomogeneous distribution of additives and large aggregates of solid LiTFSI. These aggregates make the polymer chains unpacked and inhomogeneous, which results in an amorphous film. These results are consistent with our last conclusion in UV−vis spectra; the presence of additives can affect the crystallinity of the system.

To investigate the effect of additives on the electrical properties of P3HT, the work functions (WFs) of nanocomposite films were measured. The WFs of P3HT/CNTF 0, P3HT/CNTF 1, P3HT/CNTF 2, and P3HT/CNTF 3 in environmental ambient were 4.38, 4.73, 4.78, and 4.60 eV, respectively. As expected, the addition of additives increases the charge carrier density, leading to higher WF. However, in the sample with the highest additive concentration, the WF decreases again most probably because of the loss of the crystalline order in the polymer, as suggested by other experimental findings.

Given the anisotropic properties of CNTF, its electrical resistance is dependent on the measurement orientations. In our last report, the electrical properties of CNTF in different directions were systematically investigated and analyzed.[28] The lowest electrical resistance occurs along the longitudinal direction of CNTs and it increases around ten times in the normal direction. Therefore, to increase the electrical conductivity of nanocomposite samples, all the TE measurements were performed in the direction parallel to the CNTs. Figure 4 shows the TE properties of the nanocomposite films with different amounts of dopants. The TE properties of pure P3HT (P3HT 0) and other layers with low additive content (P3HT 1 and P3HT 2) could not be measured because of their high resistances. However, the TE properties of P3HT at the highest dopant content could be measured and are shown in Figure S7. Even though the electrical conductivity of P3HT 3 has been improved several orders of magnitude compared to the pristine P3HT, it is not still conductive enough to give an acceptable power factor. Regarding the electrical conductivity, the results show that the integration of CNTF into P3HT significantly improves the electrical conductivity (Figure 4a) and reduces the Seebeck coefficient (Figure 4b).

In the case of the pristine P3HT, the electrical conductivity of the composite increases from about ~10^{-7} to 160.61 S/cm upon the addition of CNTF. Figure 4b shows that the integration of CNTF to pristine P3HT leads to the Seebeck coefficient of 26.6 μV/K. Based on the literature, the Seebeck coefficient of pristine P3HT is 1550 μV/K.[51] This reduction could be attributed to the standard trade-off between the electrical conductivity and the Seebeck coefficient. Figure 4a shows that the electrical conductivity was decreased by further addition of the dopants. The effect of doping is not simply proportional to the dopant concentration but also related to the effective dispersion in the polymer. As concentration increases, possible segregation or precipitation does not guarantee higher conductivities in P3HT/CNTF composites because the dopants might act as defects on the surface of the

https://dx.doi.org/10.1021/acsomega.0c02663
ACS Omega XXXX, XXX, XXX−XXX

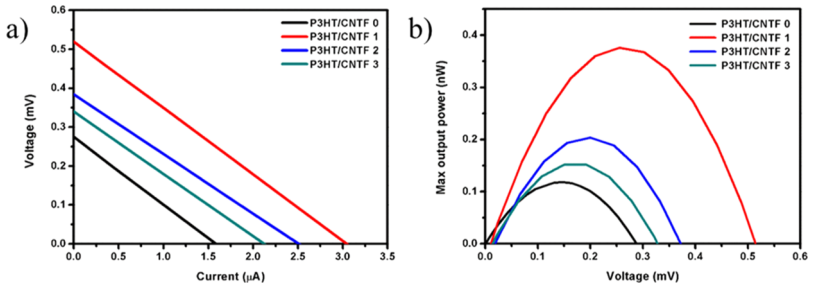

Figure 5. (a) Current−voltage and (b) power−voltage characteristics of P3HT/CNTF nanocomposites with different additive contents. All the graphs were measured at a temperature difference of 10 K.

CNTF. We believe that the electrical conductivity of the composites could be estimated based on the parallel-connected mixture model.[49] Because of the much higher electrical conductivity of CNTF than polymers, we should expect that the conductivity was mainly determined by CNTF and not by the polymers.

Interestingly, the additives improved the Seebeck coefficient in the composite. It was increased from 26.6 μV/K in P3HT/CNTF 0 to 45.9 μV/K in P3HT/CNTF 1 at room temperature.

This is an unexpected result; the trade-off relationship between the electrical conductivity and Seebeck coefficient of the conjugated polymers is well-known. They are usually inversely correlated.[24] We believe that the improvement of the Seebeck coefficient in the P3HT/CNTF 1 sample compared to the P3HT/CNTF 0 sample is related to the crystallinity and ordering of the polymer itself. As XRD patterns and UV−vis spectra showed, the additives improved the crystallinity and interchain order, which means that the charge carrier mobility was also improved. Petsagkourakis et al.[52] reported the correlation between the Seebeck coefficient and the charge carrier mobility in the polymer films. They showed that the improvement in the crystallinity and charge carrier mobility could change the slope of the density of states near the Fermi level, so the Seebeck coefficient and electrical conductivity could be simultaneously improved. Another reason might be related to the effect of CNTF on ordering. As has already been discussed, based on our analysis of UV−vis spectra, the interchain order in the composites was improved, testified by the increase in the intensity of the peak at 607 nm. Figure S2 shows that P3HT/CNTF 1 has the highest intensity of the peak at 607 nm among the different P3HT formulations. As shown in Figure 4b, with doubling and quadrupling the amount of additives, the Seebeck coefficient decreased again. The Seebeck coefficients at room temperature were 35.8 and 33.7 μV/K for P3HT/CNTF 2 and P3HT/CNTF 3, respectively. One of the plausible reasons for this decrease might be related to the morphology change. Based on the morphological characterization, increasing the dopants is associated with the appearance of larger grains. These grains and defects severely affect the charge transport, besides adversely affecting the interconnection of the polymer and CNTF. In those samples, the polymer could not surround the CNTF as uniformly as P3HT/CNTF 1. Therefore, the interlayer between them is incomplete, which badly affects the charge carrier mobility and the Seebeck coefficient.[53] Moreover, by increasing the additive content, the concentration of the charge carrier was also greatly enhanced, and based on WF results, the Fermi level goes deeper in the valence band. These phenomena could lower the Seebeck coefficient upon increasing the concentration of additives.

Figure 4c shows the power factor of the different samples. The power factor of P3HT/CNTF 0, P3HT/CNTF 1, P3HT/CNTF 2, and P3HT/CNTF 3 was 13.1, 41.9, 21.1, and 16.6 μW/m K^2 at room temperature, respectively. The P3HT/CNTF 0 sample has the highest electrical conductivity, while the maximum power factor is obtained in P3HT/CNTF 1, emphasizing the important role of additives in the TE properties of composites. All TE parameters at constant temperatures (293.15 and 344.15 K) are summarized in Figure 4d. The power factor reaches a maximum for P3HT/CNTF 1 and then it drops as the concentration of additives increases. As mentioned, because of the anisotropic properties of CNTF, its electrical resistance significantly changes in different directions. To check the effect of orientation of CNTF on the electrical conductivity of nanocomposites, the sheet resistance of P3HT/CNTF 1 was measured in parallel (standard geometry) and perpendicular to CNTF. In the perpendicular direction, the sheet resistance was about four times larger than the parallel one. Besides, the Seebeck coefficient on that direction was 36.7 μV/K. Another important feature is the effect of the TBP additive on the TE properties of nanocomposite samples. For this purpose, similar samples were fabricated without the addition of TBP in the same procedure. The electrical conductivity and the Seebeck coefficient of them were measured at room temperature. The results showed that the Seebeck coefficient of these samples was slightly decreased compared to their counterpart with TBP. The electrical conductivity was also decreased with the removal of TBP. The electrical conductivity of P3HT/CNTF 1, P3HT/CNTF 2, and P3HT/CNTF 3 samples without the addition of TBP was 79.3, 57.3, and 39.1 S/cm, respectively. These results together with photographs of pure polymer films on the glass, as shown in Figure S3, confirm the positive effect of TBP on the morphology and the electrical properties of the samples. To demonstrate the significance of our result, Table S2 summarizes the synthesis method, thickness, and TE properties of our composite, compared with similar composites. This comparison shows that with respect to the simplicity of our approach and the achieved power factor, our procedure is very efficient and effective in providing high-performance composite materials for TE applications.

To demonstrate the power generation characteristics of the P3HT/CNTF composites, the maximum output power (P_{max}) was extracted from the current−voltage (I−V) measurements of samples at a temperature difference of 10 K.

Figure 5a,b shows the I−V curves and the corresponding output powers versus open-circuit voltage of different nano-

https://dx.doi.org/10.1021/acsomega.0c02663
ACS Omega XXXX, XXX, XXX−XXX

composites at a temperature difference of 10°. The cold and hot temperatures were 14 and 24 °C, respectively. As we expected from the theoretical calculation for P_{max} ($P_{max} = V_{oc}^2/4R_{In}$, where R_{In} and V_{oc} are the internal resistance and the open-circuit voltage, respectively), the P3HT/CNTF1 gives the highest value of P_{max}. The P_{max} values of P3HT/CNTF 0, P3HT/CNTF 1, P3HT/CNTF 2, and P3HT/CNTF 3 at the temperature difference are 120, 370, 200, and 150 pW, respectively.

CONCLUSIONS

In summary, the TE properties of P3HT blended with CNTF and treated with LiTFSI/TBP dopants have been investigated. CNTF was shown to be an effective filler to significantly improve the electrical conductivity of P3HT, through the formation of an interconnected network of CNTs. Additionally, the two additives could help to improve the properties of polymer as concerns TE applications. In our study, in addition to pristine P3HT combined with CNTF, we considered three different amounts of dopants. The results of SEM measurements clearly illustrated that the addition of the dopants creates agglomerates, which might affect the TE properties. The highest power factor (110 μW/m K^2, at 344.15 K) was obtained for the sample with the lowest level of additives. To explore the effect of additives, UV−vis spectroscopy and XRD have been performed and they confirmed the improvement of the interchain order and crystallinity, respectively.

The main challenges of preparing CNT-based composites are the agglomeration and the random dispersion of CNTs within the polymer. Here, the morphological characterization showed that despite common approaches, including the physical blending of CNTs and P3HT into a solvent, and in situ polymerization of P3HT, the deposition of the polymer did not change the alignment of CNTs, which is favorable for improving the electrical properties of the composite film.

A promising direction to further improve the TE properties is the investigation of different additives and treatments. For example, to keep the morphology intact, the postprocessing approaches such as the introduction of the dopant from the vapor phase or immersion in the dopant solution could also be used as an alternative to improve the electrical properties of P3HT. Given the simplicity of our approach, a similar strategy seems appropriate to fabricate flexible and large-area TE modules.

EXPERIMENTAL SECTION

Sample Preparation. A P3HT precursor was purchased from Sigma-Aldrich in the molecular weight of 85 kDa. Lithium bis(trifluoromethanesulfonyl) imide (LiTFSI) and TBP were purchased from Sigma-Aldrich company. CNTF was provided by Solarno Inc. The preparation strategy of CNTF on glass was reported elsewhere.[28] Briefly, CNTF was pulled from their substrate with a sharp razor and then transferred onto the glass substrate. The pristine P3HT was dissolved in a 1:1 chlorobenzene/dichlorobenzene solvent mixture (10 mg in 1 mL solvent). The two additives of TBP and LiTFSI dissolved in acetonitrile (520 mg/mL) were added to the solution of P3HT. Four solutions with different additive contents were prepared and labeled P3HT 0 (pristine P3HT), P3HT 1, P3HT 2, and P3HT 3. In the case of P3HT 1, the amounts of additive for 1 mL of pristine P3HT solution were 22.8 and 24 μL for TBP and LiTFSI, respectively. These values doubled for P3HT 2 and quadrupled for P3HT 3. The P3HT solutions were deposited by spin-coating at 700 rpm for 30 s, followed by 2500 rpm for 15 s. After that, the layers were annealed at 150 °C for 10 min. The layers were labeled P3HT 0, P3HT 1, P3HT 2, and P3HT 3, like the solutions. The composite layers were obtained via a similar procedure, by depositing the polymer on the CNTF/glass. Based on the different solutions, the four different formulations of the composite were labeled P3HT/CNTF 0, P3HT/CNTF 1, P3HT/CNTF 2, and P3HT/CNTF 3. Finally, silver electrical contacts (the thickness, the distance, and the length are 80 nm, 4 mm, and 9 mm, respectively) for TE measurement were deposited onto the P3HT films via controlled thermal evaporation.

Characterization. The electrical conductivity and Seebeck coefficients of the samples were measured in a vacuum chamber using a dedicated electrical system. To measure the Seebeck coefficient and electrical conductivity, the samples were placed on the two Peltier cells that forced hot and cold temperatures on the sample edges. The hot and cold temperatures of the sample were monitored by two thermal probes (Pt100 thermistors). To improve heat conduction and temperature control between Peltier cells and the sample, a thermally conductive paste was used. The setup was equipped with a Keithley 2420 source meter and Newport 8000 temperature controller and all of these were operated with a Labview software for feedback control of hot and cold sides of the sample. Because of the low electrical conductivity of P3HT 0, P3HT 1, and P3HT 2, which were out of the measurement range of the source meter, the electrical properties of them could not be measured. The resistances of the samples were extracted from the slope of current−voltage curves at different temperatures. The temperature-dependent electrical conductivity values were calculated based on the following equation

$$\sigma = \frac{l}{Rdt}$$

where R, l, d, and t represent the resistance, the distance between the two silver electrodes, the width of the silver electrode, and the thickness of the sample, respectively. Seebeck coefficient measurements were obtained normalizing the open-circuit voltage V_{oc} measured on the sample against the temperature difference, set to 5 K. To reduce the thermal heat resistance between the sample and thermistor, a thermally conductive paste was disposed at the interface. The thicknesses of all samples were measured with a profilometer (DektakVeeco 150) in different positions, and then, the average amount was reported as the thickness. The surface morphologies of different samples were measured using a scanning electron microscope FEI Magellan 400 field emission XHR-SEM (Oxford Instrument Ltd). The absorbance spectra were measured with a spectrophotometer (BLACK-Comet UV/Vis spectrometer). As shown in Figure S1, to obtain the optical band gap, the linearity edge of absorbance is extended and intersected with the energy axis and the band gap values were evaluated using this equation.[34,54−56]

$$E_g\ (\text{eV}) = 1240/\lambda_{onset}$$

The WFs of the nanocomposite were measured using the noncontact Kelvin probe method NTEGRA instrument (NT-MDT, Russia). The data were acquired with the two-pass semicontact mode with the elevation of the cantilever at the second pass up to 80 nm to avoid the contribution of the

https://dx.doi.org/10.1021/acsomega.0c02663
ACS Omega XXXX, XXX, XXX−XXX

surface to the signal. Raman spectroscopy was performed using a Raman microscope (HORIBA LabRam Aramis) under 532 nm laser excitation.

■ ASSOCIATED CONTENT

Supporting Information

The Supporting Information is available free of charge at https://pubs.acs.org/doi/10.1021/acsomega.0c02663.

Thicknesses of different samples, absorbance and edge of absorbance of samples, Raman spectra of bare CNTF, photographs of P3HT 1 and P3HT 3 with and without TBP, normalized UV−vis absorbance spectra of all samples, optical band gap of P3HT and P3HT/CNTF samples, XRD spectra of P3HT films, TE properties of P3HT 3 at different temperatures, $I-V$ curves and the corresponding output powers of P3HT 3, and comparison of TE properties of the P3HT composite (PDF)

■ AUTHOR INFORMATION

Corresponding Authors

Andrea Reale − *Department of Electronic Engineering, CHOSE-Centre for Hybrid and Organic Solar Energy, University of Rome Tor Vergata, 00133 Rome, Italy;* orcid.org/0000-0002-9275-148X; Email: reale@uniroma2.it

Alberto Vomiero − *Division of Materials Science, Department of Engineering Sciences and Mathematics, Luleå University of Technology, 97187 LuleÅ, Sweden; Department of Molecular Sciences and Nanosystems, Ca' Foscari University of Venice, 30172 Venezia Mestre, Italy;* orcid.org/0000-0003-2935-1165; Email: alberto.vomiero@ltu.se

Authors

Saeed Mardi − *Department of Electronic Engineering, CHOSE-Centre for Hybrid and Organic Solar Energy, University of Rome Tor Vergata, 00133 Rome, Italy;* orcid.org/0000-0002-7625-1629

Khabib Yusupov − *Division of Materials Science, Department of Engineering Sciences and Mathematics, Luleå University of Technology, 97187 LuleÅ, Sweden*

Patricia M. Martinez − *NanoTech Institute, University of Texas at Dallas, Richardson, Texas 75080, United States;* orcid.org/0000-0001-5694-7883

Anvar Zakhidov − *NanoTech Institute, University of Texas at Dallas, Richardson, Texas 75080, United States;* orcid.org/0000-0003-3983-2229

Complete contact information is available at: https://pubs.acs.org/10.1021/acsomega.0c02663

Funding

This research was partially funded by the Italian Space Agency (ASI) project, "PEROSKY−Perovskite, and other printable materials for energy application in space (no. 2018-1-R.0)", University of Rome "Tor Vergata" project "THERMA-Thermal markers for the evaluation of self-heating temperature in GaN HEMTs" (grant Beyond the Borders, n. 2561) and Lazio Region project "COPPER—Progetto di Gruppo di Ricerca finanziato ai sensi della L.R. Lazio 13/08 n. 85-2017-15266".

Notes

The authors declare no competing financial interest.

■ ACKNOWLEDGMENTS

The authors would like to thank Marco Risi Ambrogioni for help with the TE measurement setup. A.V. and K.Y. acknowledge the Kempe Foundation, the Knut & Alice Wallenberg Foundation, and the LTU Lab Fund program for partial funding.

■ REFERENCES

(1) Snyder, G. J.; Toberer, E. S. Complex Thermoelectric Materials. *Nat. Mater.* **2008**, *7*, 105−114.

(2) Bell, L. E. Cooling, Heating, Generating Power, and Recovering Waste Heat with Thermoelectric Systems. *Science* **2008**, *321*, 1457−1461.

(3) Slack, G. A. New Materials and Performance Limits for Thermoelectric Cooling. *CRC Handbook of Thermoelectrics*; CRC Press, 1995; pp 407−440.

(4) Weathers, A.; Khan, Z. U.; Brooke, R.; Evans, D.; Pettes, M. T.; Andreasen, J. W.; Crispin, X.; Shi, L. Significant Electronic Thermal Transport in the Conducting Polymer Poly (3, 4-ethylenedioxythiophene). *Adv. Mater.* **2015**, *27*, 2101−2106.

(5) Hynynen, J.; Kiefer, D.; Müller, C. Influence of Crystallinity on the Thermoelectric Power Factor of P3HT Vapour-Doped with F4TCNQ. *RSC Adv.* **2018**, *8*, 1593−1599.

(6) Toshima, N. Recent Progress of Organic and Hybrid Thermoelectric Materials. *Synth. Met.* **2017**, *225*, 3−21.

(7) Chen, G.; Xu, W.; Zhu, D. Recent Advances in Organic Polymer Thermoelectric Composites. *J. Mater. Chem. C* **2017**, *5*, 4350−4360.

(8) He, M.; Ge, J.; Lin, Z.; Feng, X.; Wang, X.; Lu, H.; Yang, Y.; Qiu, F. Thermopower Enhancement in Conducting Polymer Nanocomposites via Carrier Energy Scattering at the Organic−Inorganic Semiconductor Interface. *Energy Environ. Sci.* **2012**, *5*, 8351−8358.

(9) Bounioux, C.; Díaz-Chao, P.; Campoy-Quiles, M.; Martín-González, M. S.; Goñi, A. R.; Yerushalmi-Rozen, R.; Müller, C. Thermoelectric Composites of Poly (3-Hexylthiophene) and Carbon Nanotubes with a Large Power Factor. *Energy Environ. Sci.* **2013**, *6*, 918−925.

(10) Yaghoobi Nia, N.; Lamanna, E.; Zendehdel, M.; Palma, A. L.; Zurlo, F.; Castriotta, L. A.; Di Carlo, A. Doping Strategy for Efficient and Stable Triple Cation Hybrid Perovskite Solar Cells and Module Based on Poly (3-hexylthiophene) Hole Transport Layer. *Small* **2019**, *15*, 1904399.

(11) Rodrigues, A.; Castro, M. C. R.; Farinha, A. S. F.; Oliveira, M.; Tomé, J. P. C.; Machado, A. V.; Raposo, M. M. M.; Hilliou, L.; Bernardo, G. Thermal Stability of P3HT and P3HT: PCBM Blends in the Molten State. *Polym. Test.* **2013**, *32*, 1192−1201.

(12) Miyazawa, Y.; Ikegami, M.; Chen, H.-W.; Ohshima, T.; Imaizumi, M.; Hirose, K.; Miyasaka, T. Tolerance of Perovskite Solar Cell to High-Energy Particle Irradiations in Space Environment. *iScience* **2018**, *2*, 148−155.

(13) Hong, C. T.; Kang, Y. H.; Ryu, J.; Cho, S. Y.; Jang, K.-S. Spray-Printed CNT/P3HT Organic Thermoelectric Films and Power Generators. *J. Mater. Chem. A* **2015**, *3*, 21428−21433.

(14) Lee, W.; Hong, C. T.; Kwon, O. H.; Yoo, Y.; Kang, Y. H.; Lee, J. Y.; Cho, S. Y.; Jang, K.-S. Enhanced Thermoelectric Performance of Bar-Coated SWCNT/P3HT Thin Films. *ACS Appl. Mater. Interfaces* **2015**, *7*, 6550−6556.

(15) Lim, J. A.; Kim, J.-H.; Qiu, L.; Lee, W. H.; Lee, H. S.; Kwak, D.; Cho, K. Inkjet-printed Single-droplet Organic Transistors Based on Semiconductor Nanowires Embedded in Insulating Polymers. *Adv. Funct. Mater.* **2010**, *20*, 3292−3297.

(16) Qu, S.; Yao, Q.; Shi, W.; Wang, L.; Chen, L. The Influence of Molecular Configuration on the Thermoelectrical Properties of Poly (3-Hexylthiophene). *J. Electron. Mater.* **2016**, *45*, 1389−1396.

(17) Zhang, Q.; Sun, Y.; Xu, W.; Zhu, D. Thermoelectric Energy from Flexible P3HT Films Doped with a Ferric Salt of Triflimide Anions. *Energy Environ. Sci.* **2012**, *5*, 9639−9644.

(18) Hong, C. T.; Yoo, Y.; Kang, Y. H.; Ryu, J.; Cho, S. Y.; Jang, K.-S. Effect of Film Thickness and Crystallinity on the Thermoelectric Properties of Doped P3HT Films. *RSC Adv.* **2015**, *5*, 11385−11391.
(19) Mardi, S.; Pea, M.; Notargiacomo, A.; Yaghoobi Nia, N.; Carlo, A. D.; Reale, A. The Molecular Weight Dependence of Thermoelectric Properties of Poly (3-Hexylthiophene). *Materials* **2020**, *13*, 1404.
(20) Yu, C.; Kim, Y. S.; Kim, D.; Grunlan, J. C. Thermoelectric Behavior of Segregated-Network Polymer Nanocomposites. *Nano Lett.* **2008**, *8*, 4428−4432.
(21) Moriarty, G. P.; De, S.; King, P. J.; Khan, U.; Via, M.; King, J. A.; Coleman, J. N.; Grunlan, J. C. Thermoelectric Behavior of Organic Thin Film Nanocomposites. *J. Polym. Sci., Part B: Polym. Phys.* **2013**, *51*, 119−123.
(22) Aghelinejad, M.; Leung, S. N. Fabrication of Open-Cell Thermoelectric Polymer Nanocomposites by Template-Assisted Multi-Walled Carbon Nanotubes Coating. *Composites, Part B* **2018**, *145*, 100−107.
(23) Choi, J.-H.; Hyun, C.-M.; Jo, H.; Son, J. H.; Lee, J. E.; Ahn, J.-H. Thermoelectric Elastomer Fabricated Using Carbon Nanotubes and Nonconducting Polymer. *Jpn. J. Appl. Phys.* **2017**, *56*, 095101.
(24) Glaudell, A. M.; Cochran, J. E.; Patel, S. N.; Chabinyc, M. L. Impact of the Doping Method on Conductivity and Thermopower in Semiconducting Polythiophenes. *Adv. Energy Mater.* **2015**, *5*, 1401072.
(25) Tonga, M.; Wei, L.; Wilusz, E.; Korugic-Karasz, L.; Karasz, F. E.; Lahti, P. M. Solution-Fabrication Dependent Thermoelectric Behavior of Iodine-Doped Regioregular and Regiorandom P3HT/Carbon Nanotube Composites. *Synth. Met.* **2018**, *239*, 51−58.
(26) Du, Y.; Shen, S. Z.; Yang, W. D.; Cai, K. F.; Casey, P. S. Preparation and Characterization of Multiwalled Carbon Nanotube/Poly (3-Hexylthiophene) Thermoelectric Composite Materials. *Synth. Met.* **2012**, *162*, 375−380.
(27) Peng, H.; Sun, X. Highly Aligned Carbon Nanotube/Polymer Composites with Much Improved Electrical Conductivities. *Chem. Phys. Lett.* **2009**, *471*, 103−105.
(28) Yusupov, K.; Stumpf, S.; You, S.; Bogach, A.; Martinez, P. M.; Zakhidov, A.; Schubert, U. S.; Khovaylo, V.; Vomiero, A. Flexible Thermoelectric Polymer Composites Based on a Carbon Nanotubes Forest. *Adv. Funct. Mater.* **2018**, *28*, 1801246.
(29) Ko, Y.; Kim, Y.; Lee, C.; Kim, Y.; Jun, Y. Investigation of Hole-Transporting Poly (Triarylamine) on Aggregation and Charge Transport for Hysteresisless Scalable Planar Perovskite Solar Cells. *ACS Appl. Mater. Interfaces* **2018**, *10*, 11633−11641.
(30) Juarez-Perez, E. J.; Leyden, M. R.; Wang, S.; Ono, L. K.; Hawash, Z.; Qi, Y. Role of the Dopants on the Morphological and Transport Properties of Spiro-MeOTAD Hole Transport Layer. *Chem. Mater.* **2016**, *28*, 5702−5709.
(31) Kim, H. J.; Koizhaiganova, R. B.; Karim, M. R.; Lee, G. H.; Vasudevan, T.; Lee, M. S. Synthesis and Characterization of Poly (3-octylthiophene)/Single Wall Carbon Nanotube Composites for Photovoltaic Applications. *J. Appl. Polym. Sci.* **2010**, *118*, 1386−1394.
(32) Yusupov, K.; Zakhidov, A.; You, S.; Stumpf, S.; Martinez, P. M.; Ishteev, A.; Vomiero, A.; Khovaylo, V.; Schubert, U. Influence of Oriented CNT Forest on Thermoelectric Properties of Polymer-Based Materials. *J. Alloys Compd.* **2018**, *741*, 392−397.
(33) Meng, D.; Sun, J.; Jiang, S.; Zeng, Y.; Li, Y.; Yan, S.; Geng, J.; Huang, Y. Grafting P3HT Brushes on GO Sheets: Distinctive Properties of the GO/P3HT Composites Due to Different Grafting Approaches. *J. Mater. Chem.* **2012**, *22*, 21583−21591.
(34) Dimitriev, O. P. Effect of Confinement on Photophysical Properties of P3HT Chains in PMMA Matrix. *Nanoscale Res. Lett.* **2017**, *12*, 510.
(35) Printz, A. D.; Lipomi, D. J. Competition between Deformability and Charge Transport in Semiconducting Polymers for Flexible and Stretchable Electronics. *Appl. Phys. Rev.* **2016**, *3*, 021302.
(36) Chang, J.-F.; Clark, J.; Zhao, N.; Sirringhaus, H.; Breiby, D. W.; Andreasen, J. W.; Nielsen, M. M.; Giles, M.; Heeney, M.; McCulloch, I. Molecular-Weight Dependence of Interchain Polaron Delocalization and Exciton Bandwidth in High-Mobility Conjugated Polymers. *Phys. Rev. B: Condens. Matter Mater. Phys.* **2006**, *74*, 115318.
(37) Cai, M.; Tiong, V. T.; Hreid, T.; Bell, J.; Wang, H. An Efficient Hole Transport Material Composite Based on Poly (3-Hexylthiophene) and Bamboo-Structured Carbon Nanotubes for High Performance Perovskite Solar Cells. *J. Mater. Chem. A* **2015**, *3*, 2784−2793.
(38) Bernardi, M.; Giulianini, M.; Grossman, J. C. Self-Assembly and Its Impact on Interfacial Charge Transfer in Carbon Nanotube/P3HT Solar Cells. *ACS Nano* **2010**, *4*, 6599−6606.
(39) Wang, S.; Sina, M.; Parikh, P.; Uekert, T.; Shahbazian, B.; Devaraj, A.; Meng, Y. S. Role of 4-Tert-Butylpyridine as a Hole Transport Layer Morphological Controller in Perovskite Solar Cells. *Nano Lett.* **2016**, *16*, 5594−5600.
(40) Guo, Y.; Liu, C.; Inoue, K.; Harano, K.; Tanaka, H.; Nakamura, E. Enhancement in the Efficiency of an Organic−Inorganic Hybrid Solar Cell with a Doped P3HT Hole-Transporting Layer on a Void-Free Perovskite Active Layer. *J. Mater. Chem. A* **2014**, *2*, 13827−13830.
(41) Bi, H.; Zhang, Y. Influence of the Additives in Poly (3-Hexylthiophene) Hole Transport Layer on the Performance of Perovskite Solar Cells. *Mater. Lett.* **2015**, *161*, 767−769.
(42) Kim, Y.; Yeom, H. R.; Kim, J. Y.; Yang, C. High-Efficiency Polymer Solar Cells with a Cost-Effective Quinoxaline Polymer through Nanoscale Morphology Control Induced by Practical Processing Additives. *Energy Environ. Sci.* **2013**, *6*, 1909−1916.
(43) Kumar, V.; Wang, H.; Rodenburg, C. High-Efficiency Inverted Polymer Solar Cells via Dual Effects of Introducing the High Boiling Point Solvent and the High Conductive PEDOT: PSS Layer. *Org. Electron.* **2014**, *15*, 2059−2067.
(44) Giulianini, M.; Waclawik, E. R.; Bell, J. M.; Scarselli, M.; Castrucci, P.; De Crescenzi, M.; Motta, N. Microscopic and Spectroscopic Investigation of Poly (3-Hexylthiophene) Interaction with Carbon Nanotubes. *Polymers* **2011**, *3*, 1433−1446.
(45) Du, Y.; Cai, K. F.; Shen, S. Z.; Casey, P. S. Preparation and Characterization of Graphene Nanosheets/Poly (3-Hexylthiophene) Thermoelectric Composite Materials. *Synth. Met.* **2012**, *162*, 2102−2106.
(46) Wu, M.-C.; Lin, Y.-Y.; Chen, S.; Liao, H.-C.; Wu, Y.-J.; Chen, C.-W.; Chen, Y.-F.; Su, W.-F. Enhancing Light Absorption and Carrier Transport of P3HT by Doping Multi-Wall Carbon Nanotubes. *Chem. Phys. Lett.* **2009**, *468*, 64−68.
(47) Geng, J.; Zeng, T. Influence of Single-Walled Carbon Nanotubes Induced Crystallinity Enhancement and Morphology Change on Polymer Photovoltaic Devices. *J. Am. Chem. Soc.* **2006**, *128*, 16827−16833.
(48) Saini, V.; Li, Z.; Bourdo, S.; Dervishi, E.; Xu, Y.; Ma, X.; Kunets, V. P.; Salamo, G. J.; Viswanathan, T.; Biris, A. R.; Saini, D.; Biris, A. S. Electrical, Optical, and Morphological Properties of P3HT-MWNT Nanocomposites Prepared by in Situ Polymerization. *J. Phys. Chem. C* **2009**, *113*, 8023−8029.
(49) Qu, S.; Wang, M.; Chen, Y.; Yao, Q.; Chen, L. Enhanced Thermoelectric Performance of CNT/P3HT Composites with Low CNT Content. *RSC Adv.* **2018**, *8*, 33855−33863.
(50) Hwang, S.; Potscavage, W. J., Jr.; Nakamichi, R.; Adachi, C. Processing and Doping of Thick Polymer Active Layers for Flexible Organic Thermoelectric Modules. *Org. Electron.* **2016**, *31*, 31−40.
(51) Zou, Y.; Huang, D.; Meng, Q.; Di, C.-a.; Zhu, D. Correlation between Seebeck Coefficient and Transport Energy Level in Poly (3-Hexylthiophene). *Org. Electron.* **2018**, *56*, 125−128.
(52) Petsagkourakis, I.; Pavlopoulou, E.; Cloutet, E.; Chen, Y. F.; Liu, X.; Fahlman, M.; Berggren, M.; Crispin, X.; Dilhaire, S.; Fleury, G.; Hadziioannou, G. Correlating the Seebeck Coefficient of Thermoelectric Polymer Thin Films to Their Charge Transport Mechanism. *Org. Electron.* **2018**, *52*, 335−341.
(53) Wu, R.; Yuan, H.; Liu, C.; Lan, J.-L.; Yang, X.; Lin, Y.-H. Flexible PANI/SWCNT Thermoelectric Films with Ultrahigh Electrical Conductivity. *RSC Adv.* **2018**, *8*, 26011−26019.

https://dx.doi.org/10.1021/acsomega.0c02663
ACS Omega XXXX, XXX, XXX−XXX

(54) Silva Santos, B. P.; Rubio Arias, J. J.; de Fátima Vieira Marques, M.; de Melo Furtado, J. G.; Silva, L. A.; Simão, R. A. Synthesis and Characterization of Poly (3-Hexylthiophene) for Organic Solar Cells. *Macromol. Symp.* **2019**, *383*, 1700078.
(55) Keshtov, M. L.; Kuklin, S. A.; Radychev, N. A.; Nikolaev, A. Y.; Koukaras, E. N.; Sharma, A.; Sharma, G. D. Design and Synthesis of New Ultra-Low Band Gap Thiadiazoloquinoxaline-Based Polymers for near-Infrared Organic Photovoltaic Application. *RSC Adv.* **2016**, *6*, 14893−14908.
(56) Zhang, W.; Zhu, R.; Li, F.; Wang, Q.; Liu, B. High-Performance Solid-State Organic Dye Sensitized Solar Cells with P3HT as Hole Transporter. *J. Phys. Chem. C* **2011**, *115*, 7038−7043.

https://dx.doi.org/10.1021/acsomega.0c02663
ACS Omega XXXX, XXX, XXX−XXX